Chapter 2

Literature Review

This section is classified into three categories. The first section of the literature survey comprises of two subsections. The first subsection focused on the preparation, characterisation, and thermophysical properties evaluation of hybrid nanofluid for the utilization of the composite fluid application into the heat exchanger in the tube side. Also, the next subsection contributes to the preparation, thermophysical properties evaluation of blended biodiesel to be used as fuel in the engine. The second section of the literature survey focuses on the heat transfer and pressure drop investigation of different geometry aspects of wavy fin type heat exchangers. Also, the second subsection literature review comprises experimental and numerical investigation of passive inserts as heat transfer enhancement techniques in the tube side of the heat exchanger. The third section of the literature survey focuses on the energy utilization for fuel preheating and its effect on the engine parameters.

2.1 Preparation and characterization of hybrid nanofluid

In order to get a homogenous and stable suspension for hybrid nanofluids, the technique of preparation is critical. Hybrid nanofluids have been prepared using both one-step and two-step procedures. The one-step process involves the simultaneous production and dispersion of several kinds of nanoparticles in the base fluid. In this method, the nanoparticle production and then nanofluid preparation is carried out concurrently. Nanoparticle synthesis and their dispersion into the primary fluid is completed in one go. This method is suitable for high-conductive materials to prevent oxidation. Although it is not an economical method for mass nanofluid production. The preparation of various nanoparticles is followed by dispersion in the base fluid in the two-step technique. Nanoparticle production and nanofluid preparation is produced separately. Two step technique is more suitable and economical for mass production.

To avoid agglomeration, dispersing devices like an ultrasonic disrupter, magnetic stirrer, and high-pressure homogenizer have been extensively used. Many literature studies are available on one step and two step method preparation of the nanofluid (**Wei et al., 2017**). Open research is available for the hybrid nanofluid preparation under several base fluids (**Zubir et al., 2015, Raja et al., 2016, Hayat et al., 2017, Gupta et al., 2018, Sajid et al., 2018, and Shah et al., 2019**). Hybrid nanofluid preparation available in the literature survey is presented in Table 2.1.

Table. 2.1 Different hybrid nanofluid preparation method and time.

Reference	**Nanoparticles, Particle size**	**Base fluid**	**Surfactant**	**Method and Sonication time**
Suresh et al., (2011)	Al_2O_3-Cu, Average particle size – 17nm	Water	SLS	Two-step, 6hr.
Han and Rhi (2011)	Ag- Al_2O_3, Ag: 30nm Al_2O_3: 50nm	Water	Not mentioned	Two-step, 1hr.
Chen et al., (2012)	Ag-MWCNT, Average particle size – 10nm.	Water	SLS	Two-step, 2hr.
Aravind and Ramaprabhu (2012)	Graphene-MWCNT, Average particle size-8.5nm.	EG	Not mentioned	Two-step, 3hr.
Abbasi et al., (2013)	Al_2O_3-MWCNT,	Water	Gum Arabic	Two-step, 6hr.

	Average particle size 50nm.			
Munkhbayar et al., (2013)	Ag-MWCNT, Not mentioned	Water	Not mentioned	One-step, 2hr.
Baby and Ramprabhu (2013)	Ag-MWCNT, Average particle size less than 10nm.	Ethylene Glycol.	Not mentioned	Two-step, 3hr.
Batmukh et al., (2014)	TiO_2-Ag, Average particle size 50 nm.	Water	Not mentioned	Two-step, 1hr.
Baghbanzadeh et al., (2012, 2014)	Silica-MWCNT, Average particle size 10nm.	Water	Not mentioned	Two-step, 5hr.
Li et al., (2014)	SiO_2-Graphene, Average particle size 40nm	Water	Not mentioned	Two-step, 6hr.
Luo et al., (2014)	Al_2O_3- TiO_2, Average particle size 75nm	Lubricating oil	Silane Agent	Two-step, 5hr.
Sundar et al., (2014)	ND-Nickel, Average particle size 4.5nm	Water	Not mentioned	Two-step, 2hr.
Parekh (2014)	Mn-Zn-Fe_2O_4, Average size 6nm.	Hydrocarbon oils	Oleic acid	Two-step, 1hr.
Esfe at al., (2015)	Ag-MgO, Average particle size 60nm	Water	CTAB	Two-step, 3hr.
Senthilraja et al., (2015)	Al_2O_3-CuO, Average particle size 50nm	Water	Not mentioned	Two-step, 4hr.

Shende et al., (2015)	N-rGO-MWCNT, Average particle size 80nm	Water, Ethylene glycol	SLS and PEG	Two-step, 30min
Karimi et al., (2015)	Ni- Fe_2O_4, Average particle size 8.5nm	DI Water	Tetra methyl ammonium hydroxide	Two-step, 1hr.
Harandi et al., (2016)	FMWCNTs-Fe_3O_4, Fe_3O_4: 20 to 30nm FMWCNT: 5 to 15nm	Ethylene glycol	Not mentioned	Two-step, 5hr.
Toghraie et al., (2016)	ZnO-TiO_2, particle size not disclosed	Ethylene glycol	Not mentioned	Two-step, 3hr.
Sundar et al., (2016)	ND- Fe_3O_4, particle size not disclosed	Water and Ethylene glycol	Not mentioned	Two-step, 4hr.
Hamid et al., (2017)	SiO_2-TiO_2, SiO_2: 30nm TiO_2: 50nm	Water and Ethylene glycol (60:40)	Not mentioned	Two-step, 2hr.
Nabil et al., (2017)	SiO_2-TiO_2, SiO_2: 22nm TiO_2: 30 to 50nm	Water and Ethylene glycol (60:40)	Not mentioned	Two-step, 90min.
Qing et al., (2017)	SiO_2-graphene, Graphene: 12nm SiO_2: 20nm	Naphthenic mineral oil	SDS	Two-step, 4hr.

Kannaiyan et al., (2017)	Al_2O_3-CuO, Al_2O_3: 50nm, CuO: 30nm	Water and Ethylene glycol (60:40)	Not mentioned	Two-step, 2hr.
Esfahani et al., (2018)	ZnO-Ag, ZnO: 10–30nm Ag: 30–50nm	Water	Not mentioned	Two-step, 3hr.
Leong et al., (2018)	Cu-TiO_2, Cu: 40–60nm TiO_2: <25nm	Water and Ethylene glycol (50:50)	PVP, GA	Two-step, 30min.
Akhgar and Toghraie (2018)	TiO_2-MWCNT, TiO_2: 10-25nm, MWCNT: 20-30nm	Water and Ethylene glycol (60:40)	CTAB	Two-step, 1hr.
Valan et al., (2019)	TiO_2-Ag, particle size: 10-100nm	water	SDBS and SBS	Two-step, 3hr.
Mousavi et al., (2019a)	MgO-TiO_2, MgO: 40nm, TiO_2: 50nm	Water	Not mentioned	Two-step, 2hr.
Mousavi et al., (2019b)	CuO-MgO-TiO_2, Average paticle size: 29nm.	DI Water	SDS	Two-step, 3hr.
Giwa et al., (2020)	γ - Al_2O_3-MWCNT, γ - Al_2O_3: 20-30nm, MWCNT OD:10-20nm	Water	SDS	Two-step, 4hr.

Cakmak et al., (2020)	rGO-Fe_3O_4-TiO_2, Not mentioned	Ethanol	Not mentioned	Two-step, 2hr.
Moradi et al., (2020)	TiO_2-MWCNT, TiO_2: 20-30nm, MWCNT: OD: 10-60nm	Ethylene glycol-water	Not mentioned	Two-step, 4hr.
Ahmed et al., (2021)	ZnO- Al_2O_3-TiO_2, Zno: 40nm, Al_2O_3: 30nm, TiO_2: 30nm	DI Water	Span 80	Two-step, 3hr.
Muzaid et al., (2021)	CuO-TiO_2-SiO_2, CuO: 20nm, TiO_2: 30nm, SiO_2: 40nm	Ethylene glycol	Not mentioned	Two-step, 3hr.

In the open literature presence and preparation of oxide of metal nanoparticles mixing into the base fluid to form a hybrid nanofluid are a plenty. Literature studies have mainly focused on the Al_2O_3, TiO_2, and CuO-based composites hybrid nanofluid to be utilized for practical applications. **Suresh et al. (2011)** prepared a hybrid nanofluid in the range of volume concentration (0.1% - 2%) using two step method with sodium lauric sulfate (SLS) as reducing agent and sonicated for 6hours using an ultrasonicator for homogeneous dispersion of nanoparticles into the base fluid. The stability of the colloidal mixture was controlled and obtained to be stable at pH 5.5. **Bhosale and Borse (2013)** prepared the Al_2O_3-CuO water-based hybrid nanofluid by combining equal weight of CuO and Al_2O_3 of 2.5mg in 2 litres of distilled water. The quantity was gradually increased to 0.25%,

0.5%, and 1.0% by volume. **Toghraie et al. (2016)** prepared a ZnO-TiO_2/EG hybrid nanofluid by spreading an equal volume of ZnO and titanium dioxide (TiO_2) nanoparticles up in a particular amount of liquid EG. Suspensions with volume fractions ranging from 0.0 to 3.5% were agitated for 2.5hours before being ultrasonicated at a frequency of 24kHz for 6 – 7hours. The created nanofluids were obtained to be well-spread stable, with no settling for a long period. **Nine et al. (2013)** described a low-cost, high-yield synthesis process for Cu_2O and copper nanoparticles with a size distribution of less than 30nm. Cu-Cu_2O -water hybrid nanofluid was synthesised using a wet ball milling technique. Cu_2O was synthesised by oxidising Cu into Cu_2O, producing a Cu_2O layer over Cu particles, then shattering the Cu_2O layer into a shorter particle (about 20nm). **Madhesh et al. (2014)** and **Madhesh and Kalaiselvam (2015)** synthesised Cu-TiO_2 hybrid nanofluid by uniformly dispersing titania (5g) and copper acetate (0.5g) into the base fluid water mixed with absorbic acid and sodium borohydride as dispersant and sonicated for 2hours for the homogeneity at 45°C. In the open literature, there are several works on the hybrid nanofluid preparation that are analogous, eg. **Chen et al., (2012); Balla et al., (2013); Abbasi et al., (2013); Batmunkh et al., (2014); Shende et al., (2015); Harandi et al., (2016); and Kannaiyan et al., (2017). Senthilraja et al. (2015)** prepared a stable hybrid nanofluid on dispersing Al_2O_3 and CuO in equal weight into the water base fluid, with volume concentration range 0.05% to 0.2% and sonicated for 4hours with 24kHz frequency controlled at 50°C. The prepared nanofluid obtained stable for two weeks and sedimentation was checked through ultraviolet-visible spectrophotometry. **Hamid et al. (2017)** prepared SiO_2-TiO_2 with water and ethylene glycol (60:40) as base fluid using two step method at different volume concentrations varied from 0.5 to 3%. The stability was ensured by TEM (Transmission electron microscopy). Prepared solution was sonicated for 2hours and obtained stable for 4 days. In a similar investigation, **Nabil et al. (2017)** prepared a hybrid nanofluid at a volume concentration of 0.3% to 2%, and characterization was measured using an ultraviolet-visible spectrophotometer. After 90 minutes of sonication, the

author reported more than 70% of absorbance for 336 hours of sedimentation time, and the prepared nanofluid remain stable for 14 days. **Qing et al. (2017)** prepared a hybrid nanofluid of SiO_2-graphene nanoparticles dispersed into naphthenic mineral oil using two step technique and sonicated for 4hours to obtain homogeneous and stable fluid with varied volume concentrations from 0.01% to 0.08%. The author reported pH levels 9-11 were the most suitable while pH 12 was the least suitable hybrid nanofluid at higher concentrations. Also, UV – Vis. spectrophotometer and zeta potential were used to investigate the stability and obtained 14 days of stability before commencing of the sedimentation.

There are many factors that affects the agglomeration of the nanoparticles. Different measurement techniques such as UV-vis. spectrophotometer, scanning electron microscopy (SEM), Energy-dispersion X-Ray spectroscopy (EDX), Transmission electron microscopy (TEM) **(Esfahani et al., 2018; Valan et al., 2019; Giwa et al., 2020)** used to measure the sedimentation, stability and particle size of the agglomeration of the nanoparticles. Also, photographic capturing, and X-Ray diffraction the technique to observe the sedimentation and stability of the nanoparticles **(Asadi et al., 2018; Xian et al., 2020).** In the latest study, the researcher has focused on mixing three different nanoparticles into the base fluid at lower volume concentration and obtaining a higher thermophysical property with good stability due to the synergic effects. **Mousavi et al. (2019b)** prepared a ternary hybrid nanofluid at different volume concentrations in the range of 0.1 to 0.5% using sodium dodecyl sulfate (SDS) surfactant and sonicated it for 150 minutes. The morphology of the composites and stability were analyzed using TEM, EDX, SEM, and XRD images. The author reported that the prepared hybrid nanofluid at 0.1% composition remains stable for 30 days and with the highest concentration of 0.5% the sedimentation is faster and remains unstable after 3 days. **Cakmak et al. (2020)** also prepared ternary hybrid nanofluid (rGO-Fe_3O_4-TiO_2/Ethanol) using two step method and revealed that it is more stable than the reduced graphene oxide (rGO)-ethanol, better stability is caused due to bond formation occurred in

presence of Fe_3O_4 and TiO_2 nanoparticles and get decorated on the outer surface of the reduced graphene oxides that prevents the layers of rGO for overlying and heaping. **Ahmed et al. (2021)** prepared a ZnO- Al_2O_3-TiO_2/DI water at different concentrations of 0.025, 0.05, 0.075 and 0.1%. The author commercially purchased nanoparticles and mixed them into the base fluid water with 5ml of span80 as a surfactant mixed using a magnetic stirrer for 3hours and then for deagglomeration the solution is sonicated for 3hr for cell disruption. The morphology of the prepared hybrid nanofluid solution was measured through SEM, EDX, and UV-Vis spectroscopy. The photo-capturing method and pH measurement reveals that the prepared solution was long stable for 14 days at a lower concentration.

2.2 Thermophysical properties-based hybrid nanofluids

To study the thermal and hydraulic performance, the thermophysical properties plays a crucial role to justify the suitability of the working fluid to be utilized for practical applications. The thermophysical properties include thermal conductivity, dynamic viscosity, specific heat capacity, and the density of the fluid. Heat transfer depends upon the thermal conductivity and specific heat capacity of the hybrid nanofluid while pressure drop depends upon the dynamic viscosity and hybrid nanofluid density. In the open, literature empirical correlations as well as the experimental results are available to determine the thermophysical properties of the nanofluid/hybrid nanofluid (**Suresh et al., 2011; Chen et al., 2012; Baghbanzadeh et al., 2014**). In this section, the effect of nanoparticle addition on the thermophysical properties is presented. Several researchers developed an empirical and experimental correlation for the desired investigated properties.

2.2.1 Thermal conductivity of the hybrid nanofluid

The thermal conductivity of the nanofluid is a crucial parameter for heat transfer applications and thermal systems. A better heat transfer agent must have higher thermal

conductivity than a conventional fluid. The thermal conductivity of the hybrid nanofluid can be measured using different techniques and instruments. Transient hot wire method, 3ω technique, steady state parallel plate, and thermal constant analyzer. In the transient hot wire method, a heat pulse is introduced at one needle, and on the other needle which is kept in contact with the nanofluid temperature properties are measured before and after the introduction of the heat pulse. In the thermal constant analyzer, which operates on the principle of the transient plane source method, the hot disc raised the temperature, and the resistive thermometer measured with time. In a steady-state parallel plate, two similar copper plates are placed in the fluid sample and the temperature is raised, the thermal conductivity is measured using a 1-D conduction equation. The summarized thermal conductivity correlation of hybrid nanofluid is listed in the Table 2.2.

Table. 2.2 Summarized thermal conductivity correlations of hybrid nanofluids.

References	**Hybrid Nanofluids**	**Variables (T, ϕ)**	**Correlations**
Takabi and Saleh (2014)	Al_2O_3-Cu/ Water	T=27°C ϕ=0.1-3%	$\frac{k_{nf}}{k_{bf}}=\frac{\frac{\phi_{p1}k_{p1}+\phi_{p2}k_{p2}}{\phi}+2(1-\phi)k_{bf}+2(\phi_{p1}k_{p1}+\phi_{p2}k_{p2})}{\frac{\phi_{p1}k_{p1}+\phi_{p2}k_{p2}}{\phi}+2(1+\phi)k_{bf}-2(\phi_{p1}k_{p1}+\phi_{p2}k_{p2})}$
Esfe et al., (2015a)	TiO_2-Cu /Water	T=30-60°C ϕ=0.1-2%	$\frac{k_{nf}}{k_{bf}}=1.07+0.000589T-\frac{0.000184}{T\phi}+$ $4.44T\phi\cos\begin{pmatrix}6.11+0.00673T+\\4.41T\phi-0.0414\sin(T)\end{pmatrix}-32.5\phi$
Esfe et al., (2015b)	Al_2O_3-MWCNT/ Water	T=28-60°C ϕ=0-1%	$\frac{k_{nf}}{k_{bf}}=1.05+0.005T+0.06\phi+0.0099\phi T+$ $0.00317T^2+0.026\phi^2+0.034T^2\phi+0.073T\phi^2$
Toghraie et al., (2016)	TiO_2-ZnO / Water	T=25-50°C ϕ=0.1-3%	$\frac{k_{nf}}{k_{bf}}=1+0.004503\phi^{0.8717}T^{0.7972}$

Harandi et al., (2016)	MWCNT-Fe_3O_4/ Water	T=25-50°C ϕ=0.12-3%	$\frac{k_{nf}}{k_{bf}} = 1 + 0.0162\phi^{0.7038}T^{0.6009}$
Hamid et al., (2017)	TiO_2-SiO_2 /EG Water (40:60)	T=30-70°C ϕ=0-3%	$\frac{k_{nf}}{k_{bf}} = (1+\frac{\phi}{100})^{5.25}(1+\frac{T}{70})^{0.076}$
Nabil et al., (2017)	SiO_2-TiO_2 /Water EG (60:40)	T=30-80°C ϕ=0.5-3%	$\frac{k_{nf}}{k_{bf}} = (1+\frac{\phi}{100})^{5.5}(1+\frac{T}{80})^{0.01}$
Akilu et al., (2017)	TiO_2-CuO /EG	T=25-60°C ϕ=0.5-2%	$\frac{k_{nf}}{k_{bf}} = 1 + 6.2299(\frac{\phi}{100})^{0.9371}(\frac{T}{333})^{10.2685}$
Rostamian et al., (2017)	CNT-TiO_2 /Water EG (60:40)	T=20-50°C ϕ=0.02-0.75%	$\frac{k_{nf}}{k_{bf}} = 1 + 0.04056\phi T - 0.003252(\phi T)^2$ $+0.001431(\phi T)^3 - 0.000001431(\phi T)^4$
Asadi et al., (2018)	Al_2O_3-MWCNT/ Oil	T=25-50°C ϕ=0.125-1.5%	$\frac{k_{nf}}{k_{bf}} = 0.1534 + 0.00026T + 1.1193\phi$
Parsian et al., (2018)	Al_2O_3-Cu /EG	T=25-50°C ϕ=0.125-2%	$\frac{k_{nf}}{k_{bf}} = \frac{(9.6128+\phi)}{9.3885 - 0.00010759T^2} - \frac{0.0041099}{\phi}$
Moldoveanu et al., (2018)	Al_2O_3-SiO_2/Water	T=25-50°C ϕ=0.1-3%	$k_{nf} = 0.607 - 0.005\phi_1 + 0.009\phi_1^2 + 0.109\phi_2$ $-0.059\phi_2^2 + 0.013\phi_2^3$

Hamid et al., (2018)	SiO_2-TiO_2 /Water EG (60:40)	T=30-80°C VR=0.25-4%	$\frac{k_{nf}}{k_{bf}} = 1.17(1+VR)^{-0.1151}\left(\frac{T}{80}\right)^{0.0437}$, where VR is volume ratio.
Mousavi et al., (2019)	CuO-MgO-TiO_2/ Water	T=25-50°C ϕ=0.1-0.5%	$\frac{k_{nf}}{k_{bf}} = 0.7276 - \frac{9.68}{T} + \frac{283}{T^2} - \frac{4718}{T^3} + \frac{43232.4}{T^4} + 274.27\phi - 159781\phi^2 + 41691\phi^3 - 3.64\phi^4$
Taherialekouhi et al., (2019)	Graphene Oxide-Al_2O_3/ Water	T=25-50°C ϕ=0.1-1%	$\frac{k_{nf}}{k_{bf}} = 1.006 + 0.0031T^{1.185}\phi^{0.863}$
Cakmak et al., (2020)	rGO-Fe_3O_4-TiO_2/ EG	T=30-60°C ϕ=0.05-0.25%	$k_{nf} = 0.255 + 0.0701\phi$ at 30°C $k_{nf} = 0.263 + 0.0829\phi$ at 40°C $k_{nf} = 0.266 + 0.0879\phi$ at 50°C $k_{nf} = 0.271 + 0.103\phi$ at 60°C
Moradi et al., (2020)	TiO_2-MWCNT/ Water	T=20-60°C ϕ= 0.074-1%	$\frac{k_{nf}}{k_{bf}} = 1.006 + 0.0187T^{0.6719}\phi^{0.6913}$
Dezfulizadh et al., (2021)	Cu-SiO_2-MWCNT/ Water	T=30-65°C ϕ= 1-3%	$k_{nf} = 0.397 + 0.009772T + 0.3658\varphi - 0.000151T^2 - 0.1652\phi^2 + 0.00002(T^3 + T^2\phi) + 0.0286\phi^3 - 0.001603T\phi + 0.00481T\phi^2$
Yang et al., (2021)	MWCNT-TiO_2-ZnO/DW	T=30-65°C ϕ=1-3%	$k_{nf} = 0.4761 - 0.0986\phi + 0.001754T + 0.001851T\phi - 0.00001036$

Different researchers have investigated the thermal conductivity and also state the reason for the enhancement of the thermal conductivity in presence of nanoparticles. The possible reason for the enhancement of the thermal conductivity is shown in Fig. 2.1. However, an exact single

and prominent reason for the thermal conductivity enhancement is not available yet. The possible reason for the conductivity enhancement in the nanofluid is due to random motion and micro convection of the nanoparticles (**Abbasi et al., 2013; Takabi et al., 2014; Sarkar et al., 2015; Sundar et al., 2018**). Increased surface area (**Leong et al., 2018**), nanoparticles get cluster form with a liquid thin decorated over the surface, increased solid-to-solid and solid-to-liquid collision at the higher temperature (**Harandi et al., 2017**) and nanoparticles dispersion into the base fluid layer over the fluid sublayer (**Karimi et al., 2015**), with further increment due to addition of nanoparticles in addition to hybrid nanoparticles steeps the diffusive conduction with the synergetic effect (**Dezfulizadh et al., 2021**).

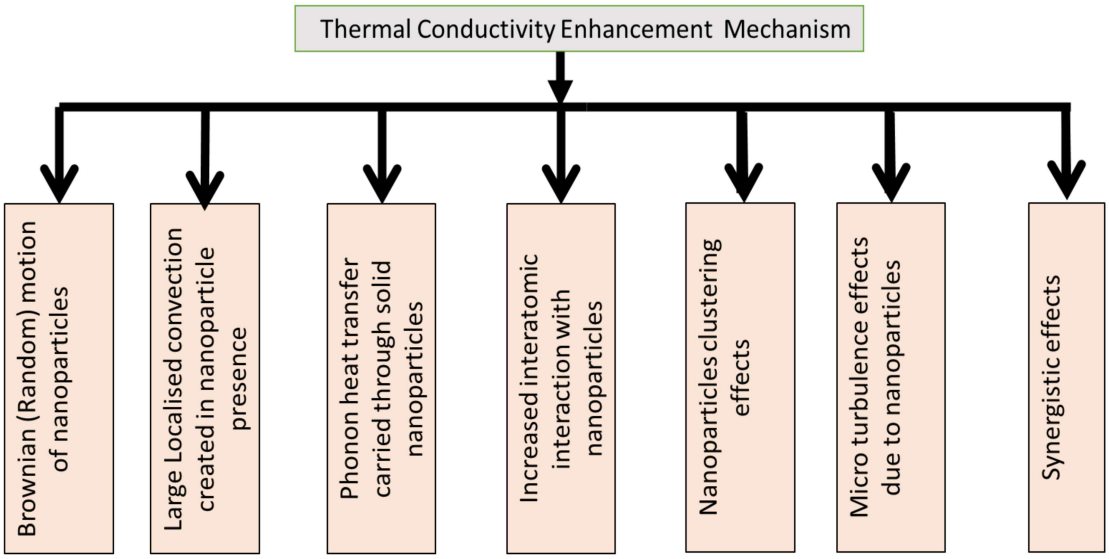

Fig. 2.1. Various reasons for the Thermal conductivity enhancement of hybrid nanofluid.

Literature present on the thermal conductivity of metals and oxides composed of hybrid nanofluid is discussed here. **Madhesh and Kalaiselvam (2014)** investigated the thermal conductivity of hybrid nanofluid composed of copper-titania with concentration and temperature as a variable parameter using a KD2 pro device and obtained the highest thermal conductivity of 0.69W/mK at a concentration of 1% an absolute temperature 353K. **Esfe et al. (2015),** proposed that with silver and magnesia dispersed into a hybrid nanofluid the thermal conductivity raises by 8.6% at a volume concentration of 0.02%. In an investigation of **Suresh et al. (2011)**, reported

that alumina-copper-based hybrid nanofluid shows higher thermal conductivity than alumina-based mono nanofluid with an optimum enhancement of 12% in thermal conductivity. **Nabil et al. (2017)**, investigated silica-titania with water and EG as base hybrid nanofluid and found a maximum of 22.8% higher thermal conductivity than ordinary fluid using a KD2 pro thermal analyzer. **Nagarajan et al. (2020)** determined the thermal conductivity using the KD2 pro device of an alumina silica-based hybrid nanofluid and reported a net 78.32% higher thermal conductivity at the fluid temperature of 60°C at a volume concentration of 0.2%. Several investigations reported higher thermal conductivity to the mono nanofluid (**Takabi and Saleh et al., 2014; Luo et al., 2014; Senthilraja et al., 2015, Valan et al., 2019; Giva et al., 2020**).

However, the nanoparticle concentration as well as the nanofluid working temperature also plays the improvement in thermal conductivity. **Esfahani et al. (2018)** calculated the effect of temperature and nanoparticle addition on the thermal conductivity of the hybrid nanofluid composed of zinc oxide and silver nanoparticles and reported that elevated temperature and higher concentration significantly increased the thermal conductivity. **Batmukh et al. (2014)** also investigated the temperature effects and nanoparticles addition to the Titania-silver hybrid nanofluid and reported with the increased temperature to 40°C with 0.2% concentration, the thermal conductivity increased from 0.60 to 0.629W/mK. The increased temperature reduces the interfacial resistance of the fluid and solid nanoparticles. **Senthilraja et al. (2015)** evaluated the thermal conductivity of mono and hybrid nanoparticles of alumina and copper oxides with temperature and volume concentration. The author reported due to an increased temperature of 60°C, the thermal conductivity of Al_2O_3-CuO/Water found 9.8%, CuO/Water is 7%, and Al_2O_3/Water showed 6.2% higher thermal conductivity than ambient temperature.

In a recent investigation ternary hybrid nanofluid shown better heat transfer agent than mono nanofluid mainly due to the hybridization of nanoparticles with unique properties. **Mousavi et al. (2019b)** investigated a ternary hybrid nanofluid composed of CuO-MgO-TiO_2/water and

reported that at a low concentration of 0.12% and temperature 50℃, the thermal conductivity of hybrid nanofluid is 38.2% higher with high concentration under normal condition. The thermal conductivity remains varied linearly with the temperature and volume concentration and with hybridization the interfacial resistance between fluid and solid gets lower. **Cakmak et al. (2020)** investigated the thermal conductivity of a hybrid nanofluid of rGO-Fe_3O_4-TiO_2/ EG composition as a function of temperature and volume concentration using KD2 pro Decagon device. The optimum thermal conductivity enhancement found to be 13.28% at 0.25% concentration. **Dezfulizadh et al. (2021)** prepared Cu-SiO_2-MWCNT/water ternary nanofluid at different concentrations and temperatures. The author obtained a maximum thermal enhancement of 14% at an elevated temperature of 65℃ with 3% volume concentration due to Brownian motion with quasi-formation of nanoparticles into the base fluid. Several researchers focused on the thermal conductivity evaluation of prepared hybrid nanofluid (**e.g. Parakh et al., 2014; Mousavi et al., 2019; Boroomandpour et al., 2020; Ahmed et al., 2020; Muzaidi et al., 2021**). Table 2.2 presents the correlation of thermal conductivity reported by various authors of hybrid nanofluids based on temperature and volume concentration. **Sahoo (2020)** investigated a ternary hybrid nanofluid with thermal conductivity which depends upon the nanoparticle morphology (spherical, platelet, and cylindrical), nanoparticle type, and individual volume concentration of the nanoparticle. Thus, the effective thermal conductivity of hybrid nanofluid is evaluated as,

$$\phi k_{hnf} = \phi_1 k_{nf,1} + \phi_2 k_{nf,2} + \phi_3 k_{nf,3} \tag{2.1}$$

Where, $k_{nf,i}$ is thermal conductivity, for the mono nanofluid for total volume fraction consisting of i^{th} (i= 1, 2, or 3) kind of suspended nanoparticle into the base fluid with $\phi = \phi_1 + \phi_2 + \phi_3$. Nanofluid conductivity of the i^{th} kind of nanoparticle (of required shape) spread are determined respectively,

$$\frac{k_{nf,i}}{\alpha_{pf}} = \frac{k_{p,i} + (\zeta_i - 1)k_{bf} + (\zeta_i - 1)\phi_i (k_{p,i} - k_{bf})}{k_{p,i} + (\zeta_i - 1)k_{bf} - \phi_i (k_{p,i} - k_{bf})} \tag{2.2}$$

Where the empirical shape coefficient, ζ , for represents different shapes of nanoparticles. The thermal conductivity of fluid indicates the suitability of fluid to be used for heat transfer purposes.

2.2.2 Dynamic viscosity/ viscosity of the hybrid nanofluid

Dynamic viscosity is an important parameter of a nanofluid on which the pumping power and the pressure drop are directly dependent. On the common state, precisely, the viscosity of nanofluid depends upon the nanoparticles, nanoparticle's shape, base fluid in which it is dispersed, volume concentration, and the base fluid temperature. Capillary viscometer, Brookfield Viscometer (CAP 2000), DV1 digital prime viscometer, Rheometer (Anton par, LVD 111, physica, MCR), Brookfield cone and plate viscometer, LVDE rotary viscometer, vibro-viscometer are different devices that are used for measuring the hybrid nanofluid viscosity. Different models and empirical correlations are available that considered viscosity as a function of volume fraction and temperature. The hybrid nanofluid dynamic viscosity decreases with the temperature rise and increases with the addition of the nanoparticles to the base fluid. With nanoparticles addition, the surface area increases and thus causes more friction between the solid surface and the fluid and enables additional increment in the viscosity. And with the rise in temperature, weakens inter particle and molecule adhesion and brings down the viscosity (**Yarmand et al. 2016**). Particle size is also responsible for the change in viscosity, the larger the size higher the viscosity (**Afrand et al. 2016**). Several proposed a correlation for viscosity which is dependent on the nanoparticle concentration (**Wang et al., 1999; Esfe et al., 2015;**). **Akilu et al. (2018)** proposed a correlation to determine the effective viscosity of the mixture which depends upon the concentration of nanoparticles and mixture temperature. The author also investigates the shear rate to justify the Newtonian behavior of the hybrid nanofluid by means it varies a linear trend with shear stress (**Yu et al. 2009**). **Suresh et al. (2011)** investigated the viscosity of hybrid nanofluid (Al_2O_3-Cu/water) with a concentration variation of 0.1-2% and revealed that with higher concentration the viscosity increases and with mono nanofluid it is less at lower concentration and significantly difference at

higher concentration. At higher concentrations, the viscosity remains high due to agglomeration and increased hydrodynamic diameter. **Ho et al. (2010)** obtained higher viscosity of hybrid nanofluid and revealed a net triple enhancement in the viscosity. **Baghbandzadeh et al. (2012)** investigated the viscosity of hybrid nanofluid (MWCNT-TiO_2/water) with temperature and concentration variation and obtained an 8.8% increment in viscosity than mono nanofluid at elevated temperature. Several authors investigated the hybrid nanofluids viscosity with temperature and concentration as variation (**e.g., Abbasi et al., 2013; Sundar et al., 2014; Dardan et al., 2016**). **Nabil et al. (2017)** investigated the viscosity of hybrid

Table. 2.3 Summarized Dynamic viscosity correlations of hybrid nanofluids.

References	**Hybrid Nanofluids**	**Variables (T, ϕ)**	**Correlations**
Esfe et al., (2015)	Ag-MgO /Water	T=27°C ϕ=0-0.02%	$\frac{\mu_{nf}}{\mu_{bf}} = 1 + 32.795\phi - 7214\phi^2 + 714600\phi^3 - 0.1941\phi^4$
Afrand et al., (2016)	SiO_2-MWCNT / Oil	T=25-60°C ϕ=0-1%	$\frac{\mu_{nf}}{\mu_{bf}} = 0.00337 + \exp(0.07731\phi^{1.452}T^{0.3387})$
Soltani et al., (2016)	MgO-MWCNT / EG	T=30-60°C ϕ<1%	$\frac{\mu_{nf}}{\mu_{bf}} = (0.191\phi + 0.24T^{0.342}\phi^{0.473}) \exp(1.45T^{0.12}\phi^{0.158})$
Dardan et al., (2016)	Al_2O_3-MWCNT/ oil	T=25-50°C ϕ=0.0625-1%	$\frac{\mu_{nf}}{\mu_{bf}} = 1.123 + 0.3251\phi - 0.089T + 0.0025T^2 - 0.0002386T^3 + 0.9695(\frac{T}{\phi})^{0.01719}$

Nabil et al., (2017)	SiO_2-TiO_2 /Water EG (60:40)	T=30-80°C ϕ=0.5-1%	$\frac{\mu_{nf}}{\mu_{bf}} = 37(0.1+\frac{\phi}{100})^{1.59}(0.1+\frac{T}{80})^{0.31}$
Esfe et al., (2017)	CuO-MWCNT /Lubricating oil	T=5-55°C ϕ=0.05-1%	$\frac{\mu_{nf}}{\mu_{bf}} = 0.50437 + 4.388\phi - 0.0418T - 0.2669\phi T$ $+22.66\phi^2 - 0.00121T^2 + 0.003325\phi^2 T +$ $0.00332\phi T^2 - 0.00001T^3$
Esfe et al., (2018)	CuO-MWCNT /SAE oil	T=5-55°C ϕ=0-1%	$\frac{\mu_{nf}}{\mu_{bf}} = 633.838 + 280.15\phi - 38.4183T - 6.17$ $T\phi - 305.838\phi^2 + 0.8889T^2 + 0.80768\phi^2 T$ $+0.05807\phi T^2 + 166.61\phi^3 + 0.00714T^3$
Ahmadi et al., (2018)	Fe_3O_4-MWCNT/ EG	T=25-50°C ϕ=0.8-1.8%	$\frac{\mu_{nf}}{\mu_{bf}} = \frac{-2.0987 + (4.65\phi)^{0.0969} + (0.87T)^{0.2633} + 62323\phi^2}{143.1076T^2}$
Mousavi et al., (2019)	Cuo-SiO_2-TiO_2/ Water	T=25-50°C ϕ=0.1-0.5%	$\frac{\mu_{nf}}{\mu_{bf}} = 1.7366342 - 0.043695678T + 95.54\phi$ $+0.00046772T^2 - 29249.9\phi^2 + 1.349648T\phi$ $-1.6T^3 + 6832500\phi^3 - 337.97T\phi^2 - 0.01T^2\phi$
Tian et al., (2020)	Cuo-MWCNT / EG+water (70:30)	T=20-60°C ϕ=0.025-1%	$\frac{\mu_{nf}}{\mu_{bf}} = 0.5013 + 0.019722T + 4.2387\phi -$ $0.052336T\phi$
Dezfulizadh et al., (2021)	Cu-SiO_2-MWCNT/ Water	T=30-65°C ϕ= 1-3%	$\frac{\mu_{nf}}{\mu_{bf}} = -31.8563 + 0.357064T + 58.04\phi -$ $0.007089T^2 - 31.7271\phi^2 + 0.000049T^3 +$ $6.0873\phi^3 - 0.127627T\phi + 0.000456\phi T^2 +$ $0.0011539T\phi^2$

nanofluid (SiO_2-TiO_2/Water EG (60:40)) with concentration and temperature ranges 30-80°C. The author reported 56% higher viscosity at 80°C at 1% of concentration.

The author also investigated the ternary hybrid nanofluid viscosity with temperature and concentration. **Mousavi et al. (2019)** prepared a ternary hybrid nanofluid (CuO-SiO_2-TiO_2/ Water) with a volume concentration 0.1-1% with a temperature 25- 50°C and compared it with the mono nanofluid. The author reported at low concentration 0.1% and low temperature the viscosity difference between ternary hybrid nanofluid and mono nanofluid is less and remains Newtonian fluid while at higher concentrations the viscosity difference is high due to CuO nanoparticle presence. Several authors reported the same viscosity variation with nanoparticle addition and temperature variation **(e.g., Tian et al., 2020; Dezifulzadeh et al., 2021, Yang et al., 2021).** Different correlations available for the viscosity of hybrid nanofluid in terms of concentration, temperature, and viscosity ratio are summarized in Table 2.3. Different previous studies mainly focus on different types of hybrid nanofluid viscosity. Authors also focused on the nanofluid viscosity of different nanoparticle shapes (**Timofeeva et al., 2009; Sahoo 2020**) dispersed in the base fluid. **Alawi et al. (2018)** investigated the viscosity correlations with shape and surface factors. **Sahoo (2020)** investigated a hybrid nanofluid with different shapes of nanoparticles (spherical, platelet, and cylindrical). Thus, the effective viscosity of hybrid nanofluid is evaluated as,

$$\phi\mu_{hnf} = \phi_1\mu_{nf,1} + \phi_2\mu_{nf,2} + \phi_3\mu_{nf,3} \tag{2.3}$$

Where, $\mu_{nf,i}$ is the dynamic viscosity, of the individual nanofluid for total volume fraction consisting of i^{th} (i= 1, 2, 3) kind of suspended nanoparticle into the base fluid with $\phi = \phi_1 + \phi_2 + \phi_3$. Nanofluid viscosity of the i^{th} kind of nanoparticle of a particular shape is determined by,

$$\mu_{nf,i} = \mu_{bf}\left(1 + \beta_i\phi + \lambda_i\phi^2\right) \tag{2.4}$$

Where, β and λ , represents the empirical shape coefficient for different shapes of nanoparticles. The viscosity of hybrid nanofluid with lower value can reach the expectation that fulfills the requirement and make it suitable to be used in heat exchangers for heat transfer applications.

2.2.3 Density and specific heat capacity of the hybrid nanofluid

For heat transfer enhancement in a device the density and specific heat capacity of the utilized fluid plays a crucial role. **Ho et al. (2010)** investigated the specific heat capacity of alumina and phase materials with water as the base fluid. With the increase in the nanoparticle addition, the specific heat capacity (SHC) decreases. **Baghbanzadeh et al. (2012)** investigated the density of the hybrid nanofluid with water as base fluid and revealed that with an increased in temperature the density of the hybrid nanofluid decreases and increases with the addition of nanoparticles. **Labib et al. (2013)** investigated the density and viscosity of oxides nanoparticles and revealed that an increase in density is more than viscosity due to oxides nanoparticle addition. Some researcher also revealed that specific heat capacity and density increases with concentration while the specific heat increases with temperature and density decreases with an increase in temperature. **Asokan et al. (2020)** investigated the rheological properties, SHC, of hybrid nanofluid Al_2O_3-CuO in the base fluid. With the increase in temperature, the increase in temperature water hydrogen bond breaks allows increasing the SHC of the hybrid nanofluid. Several research investigations showed the same pattern of a trend with volume concentration and temperature **(Gao et al., 2019; Wole et al., 2020).** Although researcher observation differs on the nanoparticle concentration and temperature effects on SHC**,** SHC decreases with nanoparticle addition (**Yarmand et al. 2016).** As there is disparate and paucity in the available experimental research data and the density and SHC of hybrid nanofluid remain linear trends with the nanoparticle addition and temperature therefore the density of and specific heat capacity of the hybrid nanofluid is determined from the theoretical correlations. The density of the hybrid nanofluid is determined from the mass-measuring balance systems and the specific heat capacity of the hybrid nanofluid is derived from the energy balance. The density and specific heat capacity generalized equations are as follows.

$$\rho_{hnf} = \sum_{i=1}^{3} \phi_i \rho_i + (1-\phi)\rho_{bf} \tag{2.5}$$

$$\left(\rho c_p\right)_{hnf} = \sum_{i=1}^{3} \phi_i \left(\rho c_p\right)_i + \left(1-\phi\right)\left(\rho c_p\right)_{bf} \tag{2.6}$$

Here ρ represents the density, c_p is the specific heat capacity of the fluid.

2.3 Biodiesel for low grade energy utilization

Biodiesel is often made through transesterification, which produces esters and glycerol as waste by combining a lipid reaction with a catalyst (alcohol), which is the process of alcohol dissolving an ester (alcohol cleaves). With the mixture ratio of 1:3 lipid or oil to alcohol ratio, the reaction is reversible, and extra alcohol pushes the equilibrium in the forward direction (**Brito et al., 2020**). Biodiesel is a long-chain fatty acid that is generated by combining methanol or ethanol with oils in the presence of a catalyst to produce methyl ester and glycerine (**Espinosa et al. 2015**). This process is known as transesterification, and the biodiesel that results from it is known as the methyl ester. Several investigations have looked into the generation of methyl ester from jatropha oils (**Chauhan et al. 2012**), neem oils (**Balaji et al. 2015**), and orange peel oils (**Kumar et al. 2020**). The high density, high dynamic viscosity, and low calorific value of plain oil as a fuel caused these crucial concerns (**Fattah et al. 2013, Hajjari et al. 2017**). Biodiesel blends, on the other hand, are suitable for use as fuel in diesel engines due to their non-toxic, biodegradable, and low sulphur content (**Mahalingam et al. 2018**). For the manufacture of methyl ester, experimental investigations, the crucial parameter is an appropriate ethanol-to-oil ratio, adequate temperature for the chain reaction, agitation duration, speed, and catalyst quantity (**Bayindir 2010; Dhas et al. 2018; Brito et al., 2020**). When the amount of ethanol and catalyst utilized less than ideal, the formation of methyl ester was lowered, according to a literature review (**Refaat et al., 2010; Endalew et al., 2011; Suryaputra et al., 2013; Mohadesi et al. 2019**). Alkaline catalysts, like NaOH, KOH, alkaline metals, and alkaline metal carbonate, seem to be the most extensively used catalysts for the generation of biodiesel (**Effavi et al. 2018, Aboelazayem et al. 2018; Sarvanam et al.; 2020**). Their main benefit is a strong ester yield in a mild reaction. With the presence of a

catalyst, the production situations of biodiesel are possible during short reaction times (**Yan et al., 2014**). Different biodiesel formation, ethanol ratio, agitation temperature, time, alcohol, catalyst, and yield percentage for different oil is presented in the Table 2.4. Catalysts that are alkaline Due to their sensitivity as oils are excellent for oils with low fatty acid. Instead of biodiesel, greater fatty acid methyl esters are turned into soap. The fatty acid methyl esters with alkaline catalysts, result in the creation of soap, which feels a calming effect. Biodiesel, water, and glycerine are layer-wise formation and get separated easily.

Table. 2.4 Summarized biodiesel preparation using different catalyst, alcohol, agitation time, temperature and percentage yield.

References	**Oil**	**Alcohol/ oil to alcohol volume ratio**	**Catalyst**	**Agitation time/ Temperature**	**% Yield**
Keera et al., (2011)	Frying oil	Methanol/ 6:1	$NaOCH_3$	1 hour/ 60°C	93%
Farag et al., (2011)	Palm oil	Ethanol/ 3:1	CH_3SO_3H	1 hour/130°C	80%
Wang and Yu (2012)	Soyabean oil	Methanol/21:1	NaOH	4 hour/65°C	80%
Chen et al., (2012)	Olive oil	Methanol/6:1	KOH	1/2 hour/65°C	84%
Jeon et al., (2013)	Canola oil	Methanol/20:1	H_2SO_4	2 hour/ 150°C	98%
Correla et al., (2014)	Soyabean oil	Methanol/24:1	_____	8 hour/60°C	94%

Soriana et al., (2015)	Canola oil	Methanol/ 24:1	$AlCl_3$	18 hour/115°C	98%
Zhang et al. (2016)	Esterified oil	Methanol/10:1	KOH	2 hour/ 65°C	90%
Efavi et al., (2018)	Citrullus seed oil	Methanol/5:1	NaOH	1 hour/65°C	70%
Joshi et al., (2018)	Neem oil	Methanol/6:1	H_2SO_4	1.5 hour/60°C	82%
Mohadesi et al., (2018)	Cooking oil	Methanol/4:1	KOH	2 hour/ 62°C	98%
Aboelazayem et al., (2018)	Castor oil	Methanol/5.5:1	KOH	2.5 hour/ 64°C	96.8%
Sharma et al., (2019)	Waste cotton seed oil	Methanol/7:1	KOH	2 hour/ 60°C	96%
Kaisan et al., (2020)	Elaegnus seed oil	Methanol/9:1	KOH	1 hour/ 60°C	95%
Saranavan et al., (2020)	Longifolia oil	Methanol/1:0.35	KOH	½ hour/60°C	91%
Elgharbawy et al., (2021)	Palm oil	Methanol/3:1	Eutectic Solvents	1 hour/60°C	96%

2.3.1 Thermophysical properties of the biodiesel

Biodiesel is composed of a single alky with ester forming a long chain of fatty acids produced from the seed oils, waste orange peel oils, vegetable oils, and fat of animals. The use of

biodiesel at different proportions affects the properties of the prepared mixture. Properties like viscosity, and density changes drastically with the blend of the biodiesel. The density and viscosity of biodiesel are higher than the normal diesel due to the presence of fatty acids (**Abdullah et al., 2013; Phankosol et al., 2014**). Biodiesel density impacts ignition delay time by influencing the onset of dynamic injection timings in engines while the predicted density limits stay in the range of 820-900kg/m^3. Biodiesel density decreases with temperature. Viscosity is a metric indicating the resistance to fuel flowing freely at a specific temperature. Fuel with excessively low viscosity may not properly lubricate the parts of the fuel injection system. Fuel with a high viscosity requires more force to pump. Fuel temperature is a variable that affects fuel viscosity, which controls the features of how fuel spray breaks apart (**Phankosol et al., 2014; Gulum et al., 2015; Oo et al., 2015; Ivani et al., 2016; Gulum et al., 2017)**. The viscosity and the elevated biodiesel fuel temperature in the range of 30 – 60℃ accelerate the atomization of fuel, higher fuel temperature reduces the viscosity and fuel consumption reduction. Viscosity reduces with the fuel elevated temperature and improves the engine's performance. Preheated biodiesel like preheating of waste fried oil, cottonseed oil, cashew nutshell methyl ester, palm oil, and Jatropha oil ethyl ester, reduced viscosity and improves engine performance (**Pugazhvadivu et al., 2005; Augustine et al., 2012; Vedhararaj et al., 2015; Ngaraja et al., 2022; Kodate et al., 2022**). The thermophysical properties of biodiesel also depend upon the blend of methyl esters of different oils. Past research that obtains 20-30% of blends in diesel suits best in terms of thermal properties and the performance enhancement of the engine, used biodiesel like lemon peel oil 20% blend, gatta seed oil 30% blend, palm oil 30% blend. (**Subramani et al., 2018; Rajkumar et al., 2019; Ganesan et al., 2020; Nagaraja et al., 2022**).

2.4 Performance characteristics of fin and tube heat exchanger

Compact heat exchangers are extensively utilized in the automotive industry. Advanced technologies increase the thermal loads in fin and tube heat exchangers and so different thermos-fluid research requires for establishing an energy-efficient heat exchanger to avoid thermal failure. Wavy fin and tube heat exchangers, in which air travels through the wavy fin and the coolant passes through the tube, are still a superior alternative to flat fin and tube heat exchangers when conventional methods are utilized to increase performance. It has been shown that wavy fins have greater heat transfer coefficients than flat fins, and this isn't just because they have more surface area or because the air flows through them more slowly, which improves air mixing. Although pressure drop is minimal when using wavy fins, researchers also tested the effectiveness of louvered fins, H-type wavy fins, and flat fins (**Lee et al., 2012; Chen et al., 2014; Saleem et al., 2017; Guo et al., 2017**). Though wavy fin and tube configuration still attracted many researchers due to its reliability. The different geometrical design of wavy fin and tube HX of different geometrical dimensions are listed in the Table 2.5.

Table. 2.5 Different parameters of wavy fin and tube HX with operating range.

Author	**Operating parameters and their range**
	Fin pitch(mm), Transverse tube pitch (mm), Longitudinal tube pitch (mm), waffle height (mm), air velocity (m/s), number of tube row
Wang et al., (1997)	Fin pitch (1.9-3.75), number of tube row (2-5), Longitudinal tube pitch (19.05), Transverse tube pitch (33)
Wang et al., (1999)	Fin pitch (1.27-3.66), Transverse tube pitch (25.4), Longitudinal tube pitch (19.4-29.4), number of tube row (2-6), waffle height (1.32-1.68), air velocity (3-6)

Wang et al. (2000)	Fin pitch (1.7-3.11), Fin thickness (0.12), Transverse tube pitch (25.4), Longitudinal tube pitch (19.5), number of tube row (2-4), waffle height (1.1-1.7), air velocity (0.3-6.5)
Wang et al., (2001)	Fin pitch (3.04-6.3), Fin thickness (0.12-0.25), Longitudinal tube pitch (27-33), Transverse tube pitch (31-38.1), number of tube row (2-6)
Wongwises et al., (2005)	Fin pitch (3.67-5.85), Transverse tube pitch (38.1), Longitudinal tube pitch (33), number of tube row (2-5), waffle height (2.2), air velocity (2-5)
Wang et al., (2011)	Fin pitch (1.69-4.8), Transverse tube pitch (25.4-29.4), Longitudinal tube pitch (19.4-29.4), number of tube row (2-4), waffle height (1.4-2.2), air velocity (2-5.5)
Hsieh et al., (2012)	Fin pitch (2), Fin thickness (0.2), Transverse tube pitch (25.4), Longitudinal tube pitch (19.05), number of tube row (2), collar outside dia (10.42), louver pitch (2.4)
Bhuiyan et al., (2016)	Fin pitch (3.6-4.2), Transverse tube pitch (31.75), Reynolds Number (1300-3000), Longitudinal tube pitch (27.5), number of tube row (1-5), waffle height (1.8), air velocity (2-5.5)
Naqiuddin et al., (2018)	fin width (1mm), fin transverse distance (5mm),number of tube row (3), fin length (2mm)

Different dimensional details of fin and tube heat exchangers of wavy configuration reveal the utilization for practical application. Due to the wavy structure of fins the prolonged path of air, regeneration, and thinned boundary layer fluid flow on the air side enhances the heat transfer of the heat exchanger.

Many experimental studies are available on the performance parameter evaluation of HX using mono nanofluid. Although, the utilization of hybrid nanofluid as a working fluid with passive device inserts in HX is petite in the exposed literature. The passive method includes the use of fin addition, geometrical modification, and tube inserts. Its easy installation at a lower cost makes it superior and widely used. Heat transfer improvement can be achieved by increasing the heat transfer coefficient using a hybrid nanofluid and tube inserts. Hybrid nanofluid enhanced heat transfer coefficient due to higher thermal conductivity and different mechanisms (random motion of particles, inertia, synergy, thermophoresis, gravity) while tube inserts also increase heat transfer coefficient due to several mechanisms mainly radial outward motion, regeneration of boundary, swirl action). It has been obtained that the use of hybrid nanofluid increases the performance marginal while with tube inserts the heat transfer and pressure drop enhances significantly. Studies available for HX with nanofluid and inserts are listed in Table 2.6 and Table 2.7.

2.4.1 Experimental studies of HX using Mono/hybrid nanofluid as a coolant

The present section is subclassified into two categories (i) Application of mono/hybrid nanofluid in fin and tube HX and (ii) Application of different inserts in HX. Many experimental studies are available on application of nanofluid in the Heat exchanger that is discussed below.

Experimental studies performed on the automotive radiator heat exchanger is presented here. An experimental investigation was conducted by **Goudarzi and Jamali (2017)** using Al_2O_3-EG in a car radiator heat exchanger as a coolant at a lower volume concentration of 0.2% and reported a 15% more thermal performance enhancement compared to a conventional fluid of a car radiator. Alteration of nanoparticles in the base fluid can alter the thermal performance of a car radiator. **Khan et al. (2019)** conducted an experimental analysis in a car radiator heat exchanger using ZnO nanoparticle in the H_2O-EG mixture as a radiator coolant. They reported that flow rate variation leads to variation in heat transfer and particularly at a lower flow rate and nanofluid higher concentration heat transfer found higher. Several authors obtained higher heat transfer and

Performance evaluation criteria by applying nanofluid as a cooling agent into the radiator heat exchanger. Nanofluid like Al_2O_3-H_2O, Fe_2O_3-water, SiO_2-water, ZnO-water , TiO_2-water etc. (**Peygambarzadeh et al., 2012; Peygambarzadeh et al., 2013; Hussein et al., 2014; Tomar et al., 2015; Devireddy et al., 2016; Topuz et al., 2020**) as a coolant is investigated for the application in the heat exchanger**.** Hybrid nanofluid is also used for the application of coolant in the heat exchanger. The thermal performance of the heat exchanger with Al_2O_3-TiO_2/water hybrid nanofluid as a cooling agent at a volume concentration of 0.3% improved 24.2% heat transfer with overall thermal performance in the range of 1.03-1.31 **Said et al., 2019**. **Kanthimati et al. (2020)** investigated the thermal performance of heat exchanger using hybrid nanofluid and revealed 13% enhanced heat transfer successfully in presence of a hybrid coolant. Hybrid nanofluid as coolant resulted in enhanced heat transfer. Enhanced heat transfer was obtained successfully due to hybrid coolants applied in various applications like wavy fin and tube, double tube Heat exchangers (**Sahoo et al., 2017**; **Guo, 2020**; **Kanthimati et al., 2020**). Also, the experimental utilization of mono and hybrid nanofluid as a cooling agent in the HX and its outcomes are presented in Table 2.6. Moreover, the utilization of hybrid nanofluid in wavy fin and tube heat exchanger as a cooling agent is not available in the open literature.

Table. 2.6 Experimental studies HX using mono/hybrid nanofluid as coolant.

Authors	Nanofluids	Outcomes
Peyghambarzadeh et al., (2011)	Al_2O_3-H_2O	Heat transfer coefficient exceeds by 45% and Nu improved to 40% at 1% volume concentration of alumina nanoparticle within 2 to 6 l/min of CFR.
Peygambarzadeh et al., (2012)	Al_2O_3-H_2O	The author reported 14% thermal enhancement at the highest volume fraction 1% with highest penalty in pressure drop.

Peyghambarzadeh et al., (2013)	CuO- water Fe_2O_3-water	Convective heat coefficient obtained maximum 9% higher at 0.65 % concentration of the nanoparticle.
Hussein et al., (2014)	TiO_2-water SiO_2-water	Heat transfer improvement reported being 20% in the case of TiO_2 while 32% improvement claimed for silica nanofluid
Ebrahimi et al., (2014)	TiO_2-water	Titanium oxide as a nanofluid at 0.4% of volume fraction and 60°C resulted in 9.3% of heat transfer increment.
Tomar et al., (2015)	Al_2O_3-H_2O	Heat transfer Increment of 12% at 0.1% volume concentration of 40 nm alumina particle size.
Devireddy et al., (2016)	TiO_2 /water-EG	Heat transfer increased up to 37% at 0.5% volume fraction of the nanofluid. Heat transfer increases with the coolant flow rate.
Goudarzi et al., (2017)	Al_2O_3- EG	The author obtained 15% higher thermal enhancement and low friction factor at 0.1% lower volume fraction of the nanofluid.
Naraki et al., (2017)	CuO- water	Net heat transfer coefficient improves by 8% at 0.4% of volume concentration.
Salami et al., (2018)	Al_2O_3-CuO/ Water	Heat transfer increased by 11% using hybrid nanofluid at lower concentration.
Said et al., (2019)	Al_2O_3-TiO_2 / Water	The author reported PEC obtained in the range of 1.03-1.31 with a net thermal enhancement of 24.2% with 16% penalty in pressure drop at 0.3% of volume fraction.

Khan et al., (2019)	ZnO/H_2O-EG	Coolant flow rate is proportional to heat transfer and pressure drop. PEC obtained 1.05, highest at the highest 1% volume fraction.
Topuz et al., (2020)	Al_2O_3/ Water -EG (60:40)	The cooling capacity increases to 15% at lower 0.5% concentration of the nanofluid with marginal pressure drop.
Efemwenkiekie et al., (2021)	Mg-Al/ Deionised water	The author reported 13.9% heat transfer enhancement at 0.05% volume fraction of hybrid nanofluid.

2.4.2 Numerical studies on HX using mono/hybrid nanofluid

A numerical investigation of fin and tube heat exchangers utilizing several mono/hybrid nanofluids as a cooling agent for thermal and hydraulic improvement of the heat exchanger is presented in this section. The effect of nanoparticle concentration of Al_2O_3 and CuO in water based nanofluid in heat exchanger for fluid dynamic and thermal behavior is investigated using (CFD) computational fluid dynamics by **Ravikant et al., 2010.** The author reported with an increase in the concentration of the nanoparticles the local, average friction factor, and heat transfer coefficient increase with the particle addition. The researcher looked into the turbulent heat transfer properties of water-based nanoparticles of Al_2O_3, MgO, and SiO_2 at volume fractions up to 4% and reported that over 2% volume fraction, the heat transfer coefficient is enhanced, but the heat transfer efficiency decreases further than 2% due to higher density of the mixture and its viscosity, which ultimately leads to a rise in pressure drop reported by **Meriläinen et al., 2013**. In the other investigation, **Heris et al. (2014)** investigated the utilization of CuO/H_2O as a coolant in the heat exchanger of nanoparticle size of 60 nm with particle volume concentration (0.05-0.8%). The heat transfer coefficient increased with the coolant flow rate and obtained 55% higher compared

to water at 0.8% volume concentration with 28% higher pressure drop at a lower concentration. **Tomar and Tripathi (2015)** numerically investigated the heat transfer phenomenon in a fin and tube heat exchanger using Al_2O_3-H_2O as a coolant. The author revealed 12% net increment in heat transfer of Al_2O_3 nanoparticle, 40 nm particle size, obtained at 0.1% of volume concentration. Several author investigated the utilization of nanofluid in the fin and tube heat exchanger using different mono nanofluid and obtained higher thermal performance at lower volume concentrations (**Lofti et al., 2010; Peyghambarzadhe et al., 2011; Suresh et al., 2012; Labib et al., 2013; Mojarrad et al., 2013; Nieh et al., 2014; Chavan and Pise, 2014; Patil et al., 2016; Said et al., 2019**). The major heat transfer improvement occurs in nanofluid due to its thermophysical properties. Hybrid nanofluid is better than mono nanofluid due to its higher enhancement capacity. Furthermore, the utilization of several hybrid nanofluids in the heat exchanger application is particularly focused. **Kumar and sarkar (2018)** used Al_2O_3-MWCNT hybrid nanofluid as a coolant for cooling the heat exchanger using two phase mixture model approach and revealed a net 15.6% higher thermal enhancement at a lower flow rate with little rise in pumping power.

Several numerical investigation application-based mono and hybrid nanofluid utilized in heat exchanger is presented in the Table 2.7. However little study is available on the use of hybrid nanofluid in the heat exchanger as a coolant.

Table. 2.7 Numerical studies on HX using mono/hybrid nanofluid coolant.

Authors	Nanofluids	Outcomes
Ravikant et al., (2010)	Al_2O_3-CuO/ EG	The author reported that in presence of alumina and copper oxide nanoparticles the 24% and 20% net increment in heat transfer and friction factor respectively.
Peyghambarzadhe et al., (2011)	Al_2O_3/ Water	With Alumina nanofluid, as a coolant, at 1% volume fraction heat transfer improved by 46% but requires higher penalty in pressure.
Suresh et al., (2012)	Al_2O_3-Cu/ Water	The heat transfer is improved by 13.56% using hybrid nanofluid and slightly higher friction factor obtained in case of hybrid nanofluid than Al_2O_3-water nanofluid at 0.1% volume fraction, 1730 Reynolds number.
Merilainen et al., (2013)	Al_2O_3, MgO, SiO_2/ Water	Heat transfer increases with the nanoparticle addition but get higher thermal efficiency below 2% volume fraction of the nanofluid.
Sarkar et al., (2013)	Al_2O_3, TiO_2, Cu,SiC/Water	maximum enhancement of heat transfer claimed for SiC was 15.34%, TiO_2 was lowest 14.03% while an intermediate increment in heat transfer for Al_2O_3 was 14.33% at 1% of volume fraction.
Hussein et al., (2014)	SiO_2,TiO_2/Water	The thermal performance increased with the addition of nanoparticles in 1 to 2.5% of volume fraction and highest obtained 24 to 32.5% thermal enhancement using TiO_2 water based nanofluid.

Soylu et al., (2014)	Cu/Ag-TiO_2/ Water	The author reported net 26.2% higher overall thermal enhancement using 1% of Ag-TiO_2/ Water with 21% pressure drop penalty.
Vajjha et al., (2015)	Al_2O_3,CuO/ Water	At 5500 Reynolds number, the Al_2O_3- water showed 10% and CuO-water showed 8% higher heat transfer coefficient.
Garoosi et al., (2016)	Al_2O_3/ Water	The heat transfer increases 10% with the increase in temperature of hot nanofluid.
Hussein et al., (2017)	TiO_2-Water	Numerically investigated the effect of nanofluid at higher Reynolds number in turbulent regime on a circular tube. Heat transfer efficiency increses to 20% at 4% volume fraction of nanofluid.
Sahoo et al., (2017)	Al_2O_3-SiC/ EG Brine	Highest performance index is obtained using hybrid nanofluid at 0.5% volume concentration at highest coolant flow rate.
Karimi and Afrand (2018)	MgO-MWCNT/EG	Pressure drop is 25% higher and heat transfer is 10% higher in flat tube than circular tube, with a better heat exchanger when vertically located.
Keklikcioglu et al., (2019)	GnP/Water TiO_2/Water	At 7300 Reynolds number, at 1% weight fraction, the heat transfer is 2.8 and 2.15 times higher than water using GnP and TiO_2 water based nanofluid. The pressure drop is higher in the later nanofluid.
Sahoo (2020)	Al_2O_3-MWCNT-	The author reported a 17% higher heat transfer due to higher surface area of carbon nanotubes with 12% penalty in pressure drop.

	Graphene/ Water	
Ramalingam et al., (2020)	Al_2O_3-Silica/ Water-EG(3:2)	The author reported 28.4% overall thermal enhancement using hybrid nanofluid at 0.8% volume fraction with lower pressure drop.
Javadi et al., (2021)	Al_2O_3CuO/water TiO_2-Cu/water Ag-MgO/water Fe_3O_4-MWCNT/Water	With set of 0.05 to 0.20% volume fraction, hybrid nanofluid Ag-MgO/Water showed higher thermal enhancement with working range 3200 to 7300 Reynolds number. The pressure drop increased with the nanoparticle addition.

2.4.3 Different Studies on heat exchanger using several inserts

The present section focuses on the utilization of different passive device inserts for the thermohydraulic enhancement of the heat exchanger. Passive inserts are also known as turbulator inserts used for thermal enhancement. Since these inserts increase heat transfer efficiency, swirl flow production, flow continuance, lengthened residence duration, and form a secondary flow in a direction perpendicular to the flow, they are often utilized as passive heat transfer approaches (**Naik et al., 2014; Ponnada et al., 2019; Bucak et al., 2020**). Several researchers investigate the use of twisted turbulator inserts (TTI) with little geometrical alteration results to enhance heat transfer performance.

For additional heat transfer enhancement, several researchers created new perforated Twisted turbulators inserts (PTTI) of varied perforates (**Bhuiya et al., 2013; Nanan et al., 2014; Man et al., 2016; Ponnada et al., 2019**). Similar to how **Suri et al. 2017** introduced square-centered perforated twisted turbulators and compared them to the TTI, it was discovered that the HX achieved a higher heat transfer and friction factor because the perforated shape of the HX

provides swirl induction, fluid mixing, and secondary flows as opposed to the TTI, which had multiple squared perforates. The majority of researches studied the thermohydraulic properties of HX using PTTI, which showed improved heat transmission and friction factor compared to PT. Several research studies on tube inserts in the application of heat exchanger for heat transfer enhancement is presented in Table 2.8.

Table. 2.8 Different studies on the inserts in HX for thermal enhancement.

Authors	Applications	Outcomes
Eiamsa-ard et al., (2010)	Circular tube HX	Delta winglets at the core of turbulator inserts successfully achieved 40% higher thermal enhancement.
Murugesan et al., (2011)	Twisted tape with rectangular and trapezoidal cut in HX	Trapezoidal cut at the periphery of the twisted tape resulted in the highest fluid mixing and heat transfer.
Thianpong et al., (2012)	Air HX	Heat transfer, friction factor increased with the decrement in pitch ratio and increment in turbulator width compared at 6000 Reynolds number.
Salman et al., (2013)	Circular tube HX	CFD analysis revealed higher heat transfer and friction factor on increased twist ratios of twisted tape in HX using Al_2O_3-H_2O nanofluid.
Esmaelzadeh et al., (2014)	Circular tube HX	Examined thermal and hydraulic evaluation of nanofluid in HX with different tape thicknesses. Reported 34.5% more heat transfer with higher tape thickness using γ-Al2O3/water nanofluid.

Zohir et al., (2015)	Circular tube HX	In higher Reynolds number, 4000, With coiled inserts the heat transfer increased to 45% and the 40% higher pressure required at lower inserts pitch.
Sheikholeslami et al., (2016)	Typical air HX with helical turbulator	Thermal efficiency improved with the increased open area ratio
Goudarzi and Jamali (2017)	Air HX with wire coil insert	Thermal enhancement of 12% obtained using wire inserts at 0.12% of Al_2O_3-EG nanofluid with little pressure drop.
Rashidi et al., (2018)	Air HX with inserts	At a volume fraction of 0.05%, Al_2O_3-H_2O nanofluid using circular regions increased with the increased pitch ratio in air HX with inserted baffles.
Eiamsa-ard et al., (2019)	HX with DTTI	Lower pitch and lower nanoparticle concentration of TiO_2-water yield a better HX equipped with dimpled TTI.
Sajadi et al., (2020)	Air HX with TTI	The lowest twist ratio enhanced heat transfer and pressure crop, while the medium twist ratio resulted in the highest overall performance index.
Singh and Sarkar (2021)	Circular Tube HX	Investigated TTI using hybrid nanofluid (Al_2O_3-TiO_2/ water) and obtained enhanced overall performance.

A reason for choosing turbulators in small heat exchangers as a thermal enhancer is that they offer fluid flow destruction and boundary layer regeneration, which enhances heat transfer. Therefore, turbulator inserts are the better option to be used in practical applications for thermos-hydraulic performance enhancement of the heat exchanger.

2.4.4 Different studies on preheating of biodiesel

Biodiesels have higher viscosity compared to diesel. Due to the poorer thermophysical properties of biodiesel, mostly blended biodiesel with diesel has been used for practical application. Biodiesel is prepared from different oils like palm oil, jatropha seed oil, orange peel oil, etc. (**Bayindir et al., 2010; Fattah et al., 2013; Mahalingam et al., 2018; Ganesan et al., 2020**). Direct utilization of pure oil as a fuel should be avoided due to its poor fuel atomization, carbon deposition, and high pollution. The difference between diesel and biodiesel effects on engine performance could be minimized by property changes in biodiesel. This could be achieved by preheating biodiesel using a source (**Hazar et al., 2010**). Although, biodiesel blends are appropriate to be used in diesel engines as a fuel due to their non-toxic, and biodegradable content. The fuel viscosity reduces on the elevated temperature and enhances the fuel spray atomization and thus reducing the ignition delay which ultimately better the engine performance. Preheating of fuel can be done using waste heat utilization from exhaust, waste heat of radiator coolant using an intermittent heat exchanger, and from the electrical source of heating. Also, higher fuel preheating may lead to the formation of fuel vapor that may choke the fuel flow in pipes (**Pradhan et al., 2013**). The research study revealed that critical temperature enhances atomization and it is found that preheating biodiesel fuel in the range of 30–60°C accelerates atomization resulting in better thermal efficiency and fuel consumption reduction (**Ragu et al., 2010; Augustine et al., 2012; Prabhu et al., 2018**). **Purusothaman et al. (2009)** experimentally investigated the effect of performance and emissions on orange peel oil as a fuel for the engine. The author reported lower CO and HC emissions while higher NO_x emissions when orange peel oil is used. **Kodate et al. (2022)** experimentally investigated the vateria indica methyl ester as a fuel to the engine with 30-50% mixed with diesel and obtained 30% blending is best due to high thermal efficiency. **Subramani et al. (2018)** experimentally conducted an investigation of garcinia gummi gatta seed oil blend as biofuel for the engine. The author reported a decrease in BSFC when blends

concentration increases and optimum performance obtained when 30% blend is used. Also, the details study on preheating of blended biodiesels, preheating source, and effect on engine outcomes is presented in the Table 2.9.

Table. 2.9 Several studies on preheating of biodiesel.

Authors	**Biodiesel used and Preheating temperature (°C)**	**Preheating Sources**	**Engine Outcomes**
Hazar et al., (2010)	Raw Rapeseed oil (B20, B50) and 100°C	External heat source to heat the biodiesel.	At 1500RPM and 100°C fuel temperature, fuel consumption reduces and CO emissions also decreases.
Ragu et al., (2011)	Rice bran oil and 30°C-50°C	External power source	With increased temperature to 50°C, the ignition delay shortens and the better fuel mixing the BTE increased by 6.2%.
Augustine et al., (2012)	Cotton seed oil (B30) and 30°C-100°C	External power source	Above 80°C, due to vapour locking in the fuel line the BTE decreases at elevated temperature (above 80°C) but at lower preheating temperature, HC, CO emissions reduced by 16%, 13% with 11% increased NO_X due to preheating.
Pradhan et al., (2013)	Crude Jatropha oil and 27°C-85°C	Waste heat of exhaust gas	At 1500RPM, BTE increased due to preheating and BSFC reduced

			significantly. HC and CO emissions reduced by 5.64% and 7.64%.
Vedhraj et al., (2015)	Cashew nut shell oil (B30) and 40°C-80°C	External energy source of heating	At 1500RPM and 80°C, 20% increase in BTE, 66% and 52% lower HC nad CO emissions.
Prabu et al., (2018)	Palm oil (B20-B40) and 30°C-60°C	Waste heat of the exhaust gas	At 1500RPM, with B20 BTE increased by 5.1% and CO emissions reduced by 37.5% with 2% higher NO_X emissions.
Mekonen and Sahoo (2018)	Jatropha oil methyl ester (B40) 30°C-60°C	Exhaust gas recirculation	With preheating and full load on engine the BTE increased by 16% BSFC reduced by 19% with 6% lower exhaust temperature. The CO and HC reduced by 19.5%, 5% respectively with 17.4% higher NO_X than unheated diesel fuel.
Anis et al., (2019)	Waste cooking oil (B0-B100) and 30°C-70°C	External power source	50°C is the better preheating conditions at which fuel spray is better for B100. And best thermal efficiency obtained at 40°C for B30.
Kodate et al., (2021)	Dhupa seed oil (B30-B100) and 35°C-95°C	External Power heating coil	At 75% Load and 95°C fuel temperature, BTE increased by 7.4% and BSFC, HC.CO emission reduced by 26.4%, 28.8%, 42.7% compared to unheated fuel, respectively.
Kodate et al., (2022)	Vateria indica methyl ester	External heating source	With preheating and B30, the BTE increased and obtained 30.1% close to

	(B30, B50) 30°C-80°C		unheated diesel fuel.CO, HC and soot emissions are decreased by 16.2%, 34.4% and 16.5% respectively.

2.5 Highlights

From the available literature study following highlights are obtained:

- The hybrid nanofluid is more suitable for application in the heat exchanger at lower volume concentration.
- The most used nanoparticles are Al_2O_3, CuO, and TiO_2 due to their better thermophysical properties.
- Application of passive device turbulator inserts for the improvement in the performance of the heat exchanger.
- Preheating of fuel obtained using external source power for heating and the energy of exhaust gas using an intermediate tube heat exchanger.
- At elevated fuel temperature the BTE increases while HC, CO emissions reduces with an increase in NO_X emissions at 30% of biodiesel blends.

2.6 Research gaps and Scope

Based on the literature study, different research gaps are identified. To overcome it further research is essential.

- Little work is done on the use of hybrid nanofluid in the application of heat exchanger for thermal improvement.
- Little work is performed on the optimization of the wavy fin and tube heat exchanger.
- Little work is carried on the use of turbulator inserts and hybrid nanofluid in the heat exchanger for thermal improvement.

- Open literature is not available on the optimization of the geometry of turbulator inserts with fluid flow parameters.
- Open literature is not available on the orange peel oil-based biodiesel blended preheating effects on the engine performance using waste heat of hybrid nanofluid coolant.

Hence, an attempt has been done in the thesis to fulfill the research gap stated above. This thesis is primarily focused on hybrid nanofluid preparation and thermophysical properties evaluation for practical use as a coolant in the heat exchanger. Furthermore, in the thesis, the thermal performance of the heat exchanger using prepared hybrid nanofluids and with optimized tube inserts has also been studied. And at the end, the thesis aims to include the practical application and effects of preheating blended biodiesel using waste energy of coolant on the engine performance and energy distribution.

This page is left intentionally blank